Grant Brandal
e-mail: gbb2114@columbia.edu

Gen Satoh
e-mail: gs2358@columbia.edu

Y. Lawrence Yao
e-mail: yly1@columbia.edu

Mechanical Engineering Department,
Columbia University,
New York, NY 10027

Syed Naveed
Boston Scientific Corporation,
Marlborough, MA 01752
e-mail: syed.naveed@bsci.com

Beneficial Interface Geometry for Laser Joining of NiTi to Stainless Steel Wires

Joining the dissimilar metal pair of NiTi to stainless steel is of great interest for implantable medical applications. Formation of brittle intermetallic phases requires that the joining processes used for this dissimilar pair limits the amount of over-melting and mixing along the interface. Thus, because of its ability to precisely control heat input, laser joining is a preferred method. This study explores a method of using a cup and cone interfacial geometry, with no filler material, to increase the tensile strength of the joint. Not only does the cup and cone geometry increase the surface area of the interface, but it also introduces a shear stress component, which is shown to be beneficial to tensile strength of the wire as well. The fracture strength for various cone apex angles and laser powers is determined. Compositional profiles of the interfaces are analyzed. A numerical model is used for explanation of the processing parameters. [DOI: 10.1115/1.4025495]

Introduction

In order to exploit specific material properties in different places of products, it is often beneficial to join dissimilar materials. Joining dissimilar materials can help to optimize toughness, wear resistance, chemical resistance, thermal properties, hardness, flexibility, etc. Many types of dissimilar materials can be joined (ceramics, composites, and polymers), but this paper will focus on the joining of dissimilar metals.

Due to some of its unique properties, nickel titanium (NiTi) is receiving increasing use, especially in such devices. NiTi has good biocompatibility, which makes it ideal for implantable medical devices. NiTi can allow for less invasive procedures because of its shape memory effect and superelasticity. Some examples of current NiTi applications are stents, Simon vena cava vein filters, and atrial Septal defect occlusion systems [1]. Obviously, implantable medical devices are not made simply out of a single material, which is why techniques for joining NiTi to other materials must be explored. A common pair is joining nickel titanium to stainless steel (SS), using stainless steel where NiTi is unnecessary. Using stainless steel in places where shape memory and superelasticity are not required can help to reduce the part cost, as well as exploit some of the properties of the stainless steel where desired.

The process chosen for joining a dissimilar material pair is heavily dependent on the composition of the materials of interest, and also on the specifications for the finished product [2]. Possibly the simplest way to join dissimilar materials is by using adhesives. Adhesives are sensitive to temperature, and their strength heavily relies on the amount of moisture that is absorbed [3,4]. Clearly, this is not viable for implantable medical devices. When heating processes are used for joining, many dissimilar metal pairs have a tendency to form brittle intermetallic phases [5]. In response, several different methods to minimize the amount of intermetallic formation have been reported. One proposed method is to use friction stir welding. This process reaches lower temperatures, and thus may help minimize intermetallic formation [6]. Friction stir welding of magnesium and aluminum has been shown to be possible, but it was found that the hardness across the joint became twice that of the base materials [7]. Fracture occurred at the point with the highest hardness gradient. Significantly changing the material properties is undesirable, and it was also found that there was a very narrow range for working parameters (rotation speed, weld speed). Also, friction stir welding is not easily applied to the wire geometry currently of interest. Another method is to melt a filler material that is placed between the two materials, and never directly melt the base materials. When choosing a filler material, it is important that its thermal expansion properties are similar to the materials being joined, otherwise large residual stresses will form. Nickel–chromium filler materials are often used when joining stainless steels, since they have comparable thermal properties [2]. Using zinc as a filler, Mathieu was able to achieve tensile strengths of 240 MPa when joining aluminum to stainless steel [8]. But, it is also possible to take advantage of the large difference of melting temperature between these materials. Stainless steel has a much higher melting temperature than aluminum. By laser irradiating the stainless steel side, the heat will conduct across the interface and melt the aluminum [5]. This eliminates the need for a filler material, but is restricted to material pairs with large melting temperature differences.

The dissimilar metal pair of NiTi and stainless steel, which is of interest to the medical world, does not have a very large melting temperature difference. With the use of an 80 μm wide copper filler material between NiTi and stainless steel wires, Li et al. was able to achieve a tensile fracture strength of 521 MPa [9]. But without the use of a filler material, they only reached a maximum strength of 187 MPa. Since the addition of filler materials is undesirable because it causes additional biocompatibility concerns, increasing the strength of joints without using filler materials is preferred. A process for joining nickel titanium and stainless steel wires together, without using a filler material, was proposed by Satoh and Yao [10]. As noted by Bao and Yao, when scanning a laser across a material, temperature spikes will occur as the laser approaches the trailing edge [11]. At the edges of the material, the heat cannot be conducted away by surrounding material. This spatial isolation of temperature peaks is the driving force behind Satoh's method. Their process, however, is limited in that it is difficult to apply uniform heating at the interface for larger diameter wires. This paper will introduce a method that can be applied to thicker wires. In joining processes, the interface geometry can be altered to maximize the effectiveness of the process being used. For example, including an extra lip of material along the top of a seam to be electron beam welded can provide material to fill any gaps that form [12]. To evenly heat the thicker wires currently of interest, they will be rotated during laser irradiation. A cup and cone interfacial geometry was proposed by the authors in a previous work [13], and will be investigated here. This will help to keep the wires aligned during rotation, and also increase the

Manuscript received April 15, 2013; final manuscript received September 12, 2013; published online November 5, 2013. Assoc. Editor: Yung Shin.

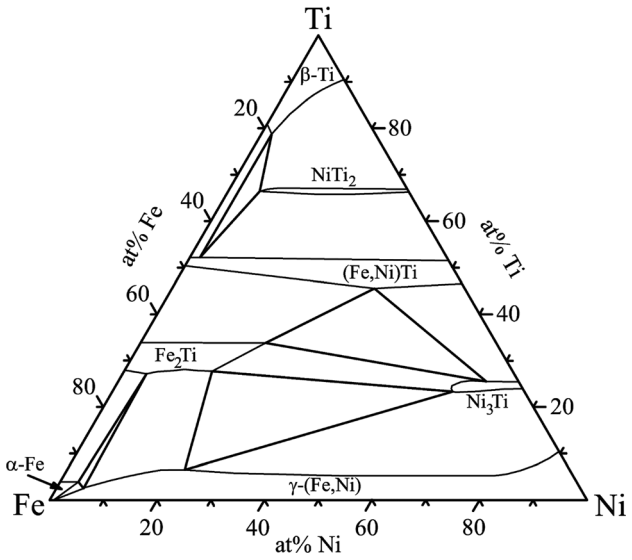

Fig. 1 Ternary phase diagram for Fe–Ni–Ti at 1173 K [13]

surface area of the interface, resulting in higher strength. The tip of the stainless steel wire is shaped into a point, and the nickel titanium is shaped as an inverted cone, whereby the stainless steel can fit into it. This results in a net increase of surface area of the interface, without increasing the outside diameter of the joint. Cones with different apex angles were analyzed. To allow for even heat distribution, the wires were rotated while being irradiated. The effect that different laser power levels had on each of these angles is presented.

Background

Ternary Phase Diagram and Brittle Intermetallics. Two of the most useful properties of nickel titanium are its superelasticity and shape memory effect. The superelasticity is due to a diffusionless martensitic transformation that occurs under large strains. This transformation is from austenitic BCC B2 into an HCP B19 crystal structure. The Clausius-Clapeyron relation indicates how, under an induced stress, martensite can form at temperatures higher than the martensite start temperature M_s [14]. During the transformation, detwinning of the martensite accommodates extensive deformation at a uniform stress. When nickel titanium has been deformed in its martensitic (low temperature) phase, heating to the austenitic phase will cause it to recover its original shape; this is the shape memory effect.

One of the biggest concerns when joining dissimilar metals is the formation of brittle intermetallic phases. Intermetallics form in very specific proportions, and have crystal structures that differ from the original base materials. Electrical, mechanical, magnetic, and chemical properties may be different from the base materials as well [15]. The specific ratios they form in makes it possible to identify phases present in a sample by using energy dispersive x-ray (EDX) analysis. Many intermetallics are subject to brittle fracture and suffer from a low crack tolerance. Their complex crystal structures have large Burgers' vectors, so it often requires less energy for fracture than for dislocation movement. A ternary phase diagram for titanium, iron, and nickel is shown in Fig. 1 [16]. This is at 1173 K, about 400 K below melting temperature for the NiTi. For simplification, we neglect the effects of the chromium that is present in the stainless steel. Chromium behaves similarly to the titanium, and there is much less of it than the other three materials [17]. Fe_2Ti is a Laves phase, and has some unique magnetic properties [18]. But, its C14 hexagonal structure is quite brittle [19]. The other common intermetallic formed is FeTi. Large regions of FeTi have been shown to decrease the tensile strength of the joint [20]. Nickel titanium and stainless steel have different thermal expansion coefficients, and van der Eijk et al. concluded that this difference could result in residual stresses and initial cracks within the intermetallic layer [21]. Using a nickel interface layer may help to lessen the amount of brittle intermetallics formed, but it will not completely prevent their formation [21]. Shortening the time period that the base materials are at or above melting temperature will limit intermetallic formation as well. Borrisutthekul et al. found that placing a heat sink with a large thermal conductivity next to the joint lowered the amount of intermetallics formed when joining steel to aluminum [22]. If over-melting occurs at the interface, iron from the stainless steel can substitute for the nickel in the NiTi's austenitic phase, lowering the martensitic start temperature M_s and allowing for the formation of an R phase [23]. This lowered M_s and decrease of nickel concentration will also result in the superelastic plateau occurring at a higher stress [14].

Phase change is not limited to the interface. The heat affected zone of the base materials will also undergo some changes. Precipitates in the base NiTi will increase, which also results in lowering the M_s temperature [24]. Once the NiTi has recrystallized, the thermodynamic parameters will remain nearly constant though [25]. Overall, to increase the fracture strength of the NiTi to stainless steel joints, it is necessary to minimize the amount of brittle intermetallic phases that form [26].

Geometrical Considerations. Characterization of the quality of each joint is based on its tensile testing results. Since the dissimilar material pair has different Young's Moduli, the stress–strain response does not have a clear, direct interpretation. Thus, the most important characteristic is the load at fracture for each joint. The fracture strength of joints can be increased by distributing the load over a larger surface area. Different interface geometries can be used to increase the contact area, without increasing the overall size of the part. Increasing the surface area will decrease the stress concentration on the interface, but sharper angles may have detrimental effects on surface wetting [27]. This places a limitation on the geometries in that they must not be too complex. One possibility is to make a U slot, and slide one piece around the other. Vaidya et al. used this method for butt welding plates of aluminum AA6605 and titanium Ti6Al4V [28]. Fracture occurred in a heat affected zone, and not at the interface itself. The simplest way to increase the interface surface area for wires is to cut the ends at an angle, in the fashion of a scarf joint. This will result in an increase of surface area, given by $A = (A_o/\cos(\varphi))$, where A_o is the cross sectional area of the wires, and φ is the angle between the normal of the surface and the longitudinal axis of the wire. This is a viable option to be applied to the 381 μm diameter wires that Satoh explored [29]. But, the wires of current interest have twice that diameter. Getting the heat to conduct through thicker wires and evenly melt the interface is not viable. Overheating must be avoided. As simply melting the base NiTi, without any mixing or intermetallic formation occurring, can decrease the tensile strength of the wire by as much as 30% [30]. One solution is to use multiple lasers, and simultaneously irradiate the top and bottom of the sample [28]. But due to the rotational symmetry of the wires, an alternative method is to use a single laser source while simultaneously rotating both of the wires during the laser scan. This paper will make use of this wire rotation.

To increase the interfacial surface area, a cup and cone geometry is proposed, as shown in Fig. 2. In a way, this is like an axisymmetric scarf joint about the longitudinal axis of the wires. The stainless steel will be shaped into a point, while the end of the NiTi is drilled out in the shape of a cone. An angle θ is defined as the apex angle of the cone. Two different apex angles will be analyzed (90 deg and 120 deg) and their strengths compared to wires without the conical interfaces. The 90 deg cones will have an interface area of 0.645 mm^2, while the 120 deg cones will be

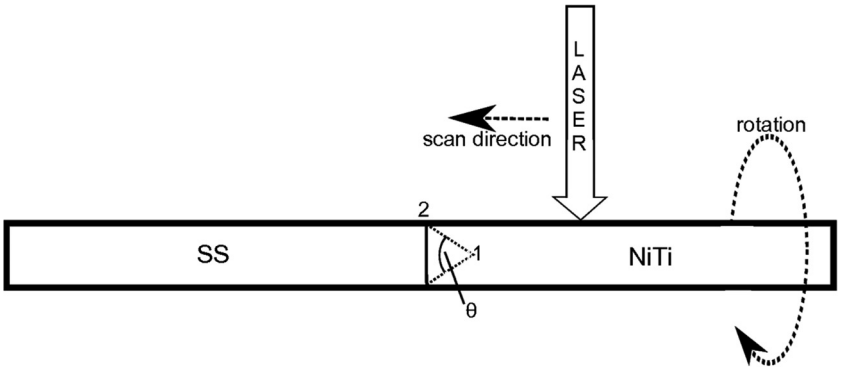

Fig. 2 Schematic diagram describing the geometry used. Point 1 is at the apex of the cone and point 2 is on the outside edge

0.527 mm^2, which are 41% and 16% larger than a flat interface, respectively. Of course, this increased surface area is not normal to the direction of loading. As such, we do not expect the effect due to this increased surface are to be equal to this same percentage increase. An additional benefit of the conical interfaces is that they help to keep the wires aligned during rotation.

Stress Intensity Formulation. Stress intensity in uniaxial tension along a crack, away from the free edges, oriented at an angle is given by [31]

$$K_{\mathrm{I}} = \sigma\sqrt{\pi a} * \sin^2\frac{\theta}{2} \tag{1}$$

$$K_{\mathrm{II}} = \sigma\sqrt{\pi a} * \sin\frac{\theta}{2}\cos\frac{\theta}{2}$$

where σ is the applied stress, a is crack length, $(\theta/2)$ is the angle between the applied load and the crack. We assume that the cracks formed will be in areas that did not melt along the interface, and also that the fracture will propagate along the joint interface within the intermetallic layer. Therefore, the cracks will be oriented $(\theta/2)$ degrees from the direction of loading as well. Figure 3 shows these K values for various interfacial angles. For an ideally brittle material, $(K_{\mathrm{IIC}}/K_{\mathrm{IC}}) = 1.2$ [32], where K_{IIC} is mode II fracture toughness and K_{IC} is mode I fracture toughness. From the graph we see that as the angle decreases (sharper cones on the wires), both K_{I} and K_{II} decrease. This effect is due to the increase of surface area on the interface. In order to exploit the higher K_{II} value, it is preferable to introduce some shear component along the joint. Figure 3 indicates that the lowest stress intensity, and therefore the strongest joints, is a result of having smaller apex angles. But, as the cone becomes sharper, heating along the interface will become less uniform, and complete joining may not be possible.

Stress singularities will form at the traction free edges of dissimilar material joints [33] and are dependent on the joining angles as well as the difference of material properties (i.e., Poisson's ratio and Young's Modulus). For a 2D plane stress situation with dissimilar materials bonded at an angle α (corresponding to $\alpha = 90\,\mathrm{deg} - (\theta/2)$, for θ defined in Fig. 2) under uniaxial tension σ_o, the stress components along the interface can be expressed as [34]

$$\sigma_\theta = 4A\left(\frac{\gamma^2}{\sin^2(\alpha)}\right)\chi_1(z,\alpha,\kappa)e^{-2\gamma z*\cot(\alpha)} + \sigma_o\sin^2(\alpha)\ \text{(normal)} \tag{2}$$

$$\tau_{r\theta} = 4B\left(\frac{\gamma^2}{\sin^2(\alpha)}\right)\chi_2(z,\alpha,\kappa)e^{-2\gamma z*\cot(\alpha)} - \sigma_o\sin(\alpha)\cos(\alpha)\ \text{(shear)}$$

where A and B are constants, $z = (r/w * \sin(\alpha))$, γ are roots of a characteristic equation, χ_i are oscillating functions, and

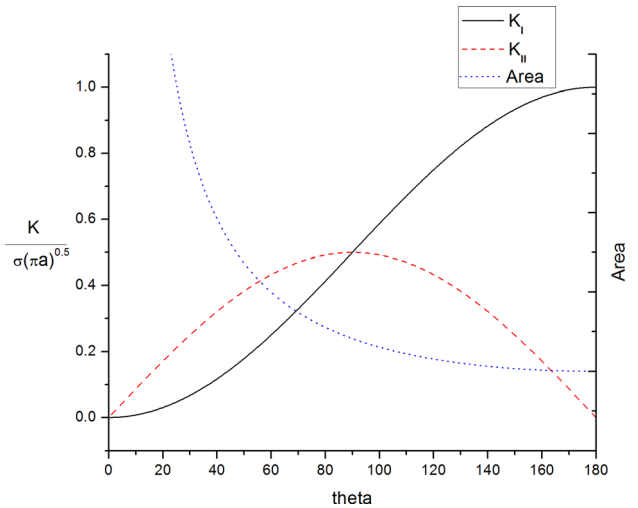

Fig. 3 Mode I stress intensity (K_{I}) and Mode II stress intensity (K_{II}) versus angle of interface, for a constant uniaxial load. The interfacial area is superimposed over-top, indicating that as the cones become sharper, the area increase results in a decrease of stress intensity.

$k = (-\gamma * \sin(\gamma)/\cos(\gamma))$. The significance of these equations is that the first term of both the normal and shear stresses contains an exponential decaying with distance from the free corner. Thus, away from the edges in the bulk of the material, the shear and normal stress components are constant for each respective interface angle. It has been shown [34] that even for very sharp angles, the stress singularity will not result in more than a 7% deviation from the uniform stress in the bulk of the material. This increase of stress at the free edge may result in failure initiating there, but due to the relatively small magnitude the benefit of introducing a shear component outweighs this effect.

Process. The NiTi is the material that will be irradiated, since it has a lower melting temperature than the stainless steel. Starting the laser a fixed distance away, and then scanning at a constant velocity toward the interface will result in heat accumulation along the interface. Once the NiTi reaches its melting temperature and joins onto the stainless steel side, the thermal conduction across the interface increases. A rapid cooling rate is desired for joining NiTi to stainless steel [29]. Since the stainless steel is at much lower temperatures than the NiTi, this desirable rapid cooling will occur. At the same time, both the wires are spun at a constant angular velocity, helping to ensure uniform heating. Along joint interfaces, the irradiated material will contract as it is cooled [12]. Since the conical portion of the NiTi encases the stainless steel, as

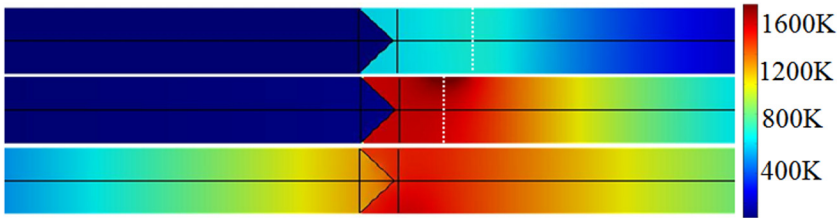

Fig. 4 Longitudinal sectioned time snapshot of thermal accumulation in 90 deg cones. Corresponding times are: (*a*) 1 s, (*b*) 4 s, and (c) 6.8 s (laser has shut off). Laser location indicated by white dotted line. Power: 15 W, angular velocity: 3000 deg/s.

this contraction occurs the NiTi will squeeze onto the stainless steel wire.

Thermal Modeling. Heat input from the laser is the only parameter we can control during the joining process, thus 3D thermal modeling was performed to help choose parameters. The heat flux of the laser was modeled as a Gaussian distribution with a spot size of 800 μm. At the interface, the initial thermal resistance is large, which results in thermal accumulation. But once the interface has melted, this resistance decreases significantly. To simulate this changing conductance across the interface, a thin thermally resistive layer was placed between the NiTi and stainless steel. By equating the heat flow in the definitions of convection and conduction heat transfer, we can get the relationship

$$h = -\frac{k}{\Delta x} \tag{3}$$

where h is the heat transfer coefficient per area, k is the thermal conductivity, and Δx is the width of the resistive layer. The non-melted NiTi-SS interface has $h = 79\,\mathrm{W/m^2K}$ [35]. Values for k and Δx were set to give this initial ratio. A temperature dependent step function was associated with Δx, so that once each node of the interface reached its melting temperature, the value of Δx would decrease, thus increasing the conductance. According to the Hagen-Ruben Relation, laser absorption can be calculated as

$$A = \sqrt{8\varepsilon_o \omega \rho} \tag{4}$$

where ε_o is the permittivity of free space, ω is the angular frequency of incident radiation, and ρ is the electrical resistivity of the material [36]. Electrical resistivity is proportional to temperature, and thus absorptivity increases as the temperature is increased. The most dramatic increase of absorptivity is when the material changes from a solid to a liquid. Since in this process melting is limited to the interface, we make the simplification of using a constant resistivity. An electrical resistivity of 5.48×10^{-7} Ω m was used, which is the value for titanium at 333 K [37]. The value for titanium is applicable since the titanium oxide layer that forms on the surface of the NiTi is similar to the surface of titanium. A laser with wavelength of 1064 nm was used, resulting in an absorptivity of 26%. Convective cooling from the argon flow is present on the outside surface of the wires. The convective heat transfer coefficient was calculated using the Zhukauskas Correlation [38]

$$\overline{\mathrm{Nu}_D} = C\mathrm{Re}_D^m \mathrm{Pr}^n \left(\frac{\mathrm{Pr}}{\mathrm{Pr}_s}\right)^{\frac{1}{4}} \tag{5}$$

$$\bar{h} = \overline{\mathrm{Nu}_D}\frac{k}{D} \tag{6}$$

where $\overline{\mathrm{Nu}_D}$ is the average Nusselt number, Re_D is the Reynolds number, Pr is the Prandtl number, k is thermal conductivity, D is the wire diameter, and C and m are constants determined from the Reynolds number. Using a kinematic viscosity for argon of 1.41×10^{-4} m^2/s [39], the Reynolds number was calculated as 0.92, resulting in $\bar{h} = 12.7\,\mathrm{W/m^2K}$. The 3D heat equation was implemented in COMSOL. Although the temperature distribution was not directly measured, the trends predicted by this thermal model will be shown to be consistent with experimental results.

Procedure

For this study, NiTi and hard tempered SS304 wires of diameter 762 μm were used. The NiTi wires had a composition of 54 at% titanium and 46 at% nickel. Initially in the austenitic phase at room temperature, the NiTi undergoes a stress induced phase transformation at 480 MPa. The angles of the points analyzed on the stainless steel samples were 90 deg and 120 deg, with corresponding values for the NiTi. In order to create the cones on the ends of the stainless steel wires, they were placed into an angled block, and then spun at 5000 rpm against 320 grit silicon carbide abrasive paper. To create the cups in the ends of the NiTi, 1143 μm diameter spot drills were used, with corresponding tip angles. After shaping, the wires were washed with acetone in an ultrasonic bath.

The NiTi wires were fastened into a rotary stage, while the stainless steel wires were placed in an un-driven ball bearing fastened onto a sliding linear stage. An axial load of 2 Newtons was applied to the linear stage. Argon was flowed into a chamber surrounding the wires at 10 scfh. A SPI redENERGY G4 fiber laser operating in CW mode at a wavelength of 1064 nm was used. Power levels of 13–17 W were analyzed in single watt increments. Laser spot size was 738 μm. The wires were rotated at angular velocities of 3000 deg/s, 2500 deg/s, and 2000 deg/s. The laser spot started 1.6 mm away from the interface, underwent 18,000 of total rotation, and stopped 0.1 mm short of the interface. This corresponds to laser irradiation times of 6 s, 7.2 s, and 9 s for 3000 deg/s, 2500 deg/s, and 2000 deg/s rotations, respectively.

Tensile testing was carried out according to ASTM E8-11 standards [40]. An Hitachi-S4700 SEM with energy dispersive x-ray spectroscopy attachment was used for the compositional analysis.

Results and Discussion

Temperature Profile. In Fig. 4, a longitudinal section view of the wires is plotted displaying temperature at three different times during the laser scan. As the NiTi wire begins to heat up, the interfacial resistance causes thermal accumulation. This indicates that most of the melting should be limited to the interface, which is desirable. If excessive melting occurred along the whole path of the laser scan, the wire would lose its structural integrity and deform. The rotation of the wires allows the hot temperature to be able to reach the extents of the NiTi cone, both points 1 and 2. Had the wires not been rotated during irradiation, insufficient heat would have been able to conduct to the apex. Once the interface has melted, the NiTi wets onto the stainless steel side, and the thermal resistivity across the interface decreases. The third time snapshot

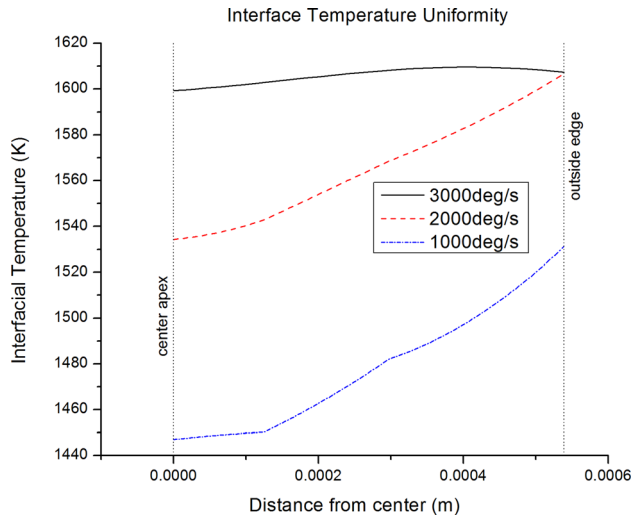

Fig. 5 Uniformity along line segment 1–2 on the interface. As the angular velocity is increased, the thermal distribution becomes more even and the average temperature rises.

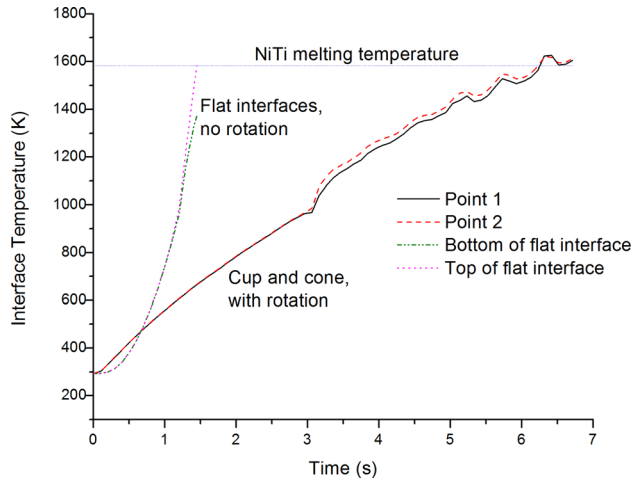

Fig. 6 Time history of points 1 and 2 along the interface from Fig. 2, compared to points at the top and bottom of the interface of wires with flat interfaces. Temperature difference between the 2 points on the rotated wires throughout the laser scan is minimal. Laser power is 15 W for the rotated wires, and 35 W for the flat interfaces.

is after wetting has occurred, and the stainless steel wire is seen to heat up.

An even temperature distribution along the interface is desired, since this will allow for uniform melting. Figure 5 displays the temperature distribution along the line segment from points 1 to 2 at the moment the laser has completed its scan. Of the three different angular velocities, 3000 deg/s has the flattest temperature distribution. It is also apparent that increasing the angular velocity increases the average temperature of the interface, despite having a shorter interaction time with the wire. As the wire is being spun faster, the input heat flux from the laser beam behaves more like a uniform ring of heat around the circumference of the wire, as opposed to a single point source. The overall power from the laser is the same, but the uniform heating may decrease the temperature gradient in the vertical direction, resulting in less heat being conducted away. Figure 6 displays the time history for points 1 and 2, and for points on the top and bottom of the interface of wires with flat interfaces that were not rotated during irradiation.

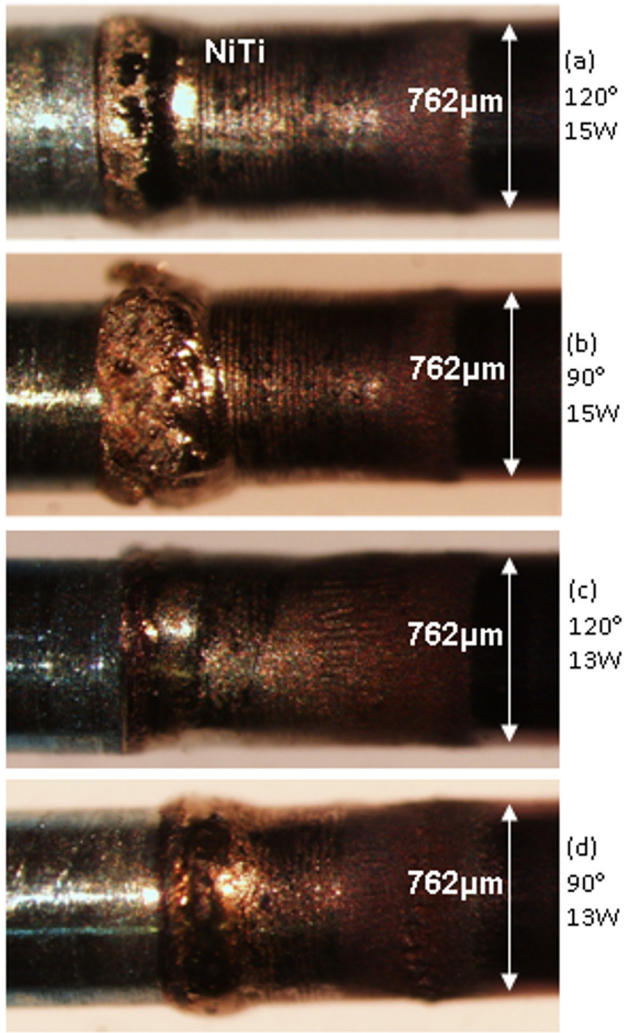

Fig. 7 Images of four different combinations of power and cone angle. The outer surface near the joint of the 90 deg wires experienced more deformation. Rotational velocity is held constant at 3000 deg/s

We are looking for the maximum temperature difference along each wire's interface. From the symmetry, the largest temperature difference on the rotated wires is between the outside point 2 and the apex point 1. For the nonrotated wires, the largest difference is between points at the top and bottom of the interface. At 1.5 s, the top of the flat wires is nearly 1700 K, while the bottom is only 1400 K. By examining longitudinally sectioned samples that were not rotated, we see that often the top is overmelted, while no melting occurs at the bottom. This is consistent with the predictions of the thermal model. If laser power is increased to allow for the bottom point to reach melting temperature, the top point will reach excessive temperatures. The temperatures at the two points on the interface that was rotated reach the melting temperature at nearly the same time, which will results in good uniformity of the joint.

Joint Morphology. Outside images of four of the joints are presented in the Fig. 7. Most apparent is the effect of thermal accumulation, in that the majority of the melting occurs in the NiTi near the interface. More melting is evident in both of the wires that are at 15 W. The interface for this power level tends to bulge out more than it does at 13 W. But for their respective power levels, the 90 deg wires tend to have a larger belled region than the 120 deg wires do. The cone is deeper in the 90 deg wires, so the walls near the end of the NiTi are much thinner for a longer

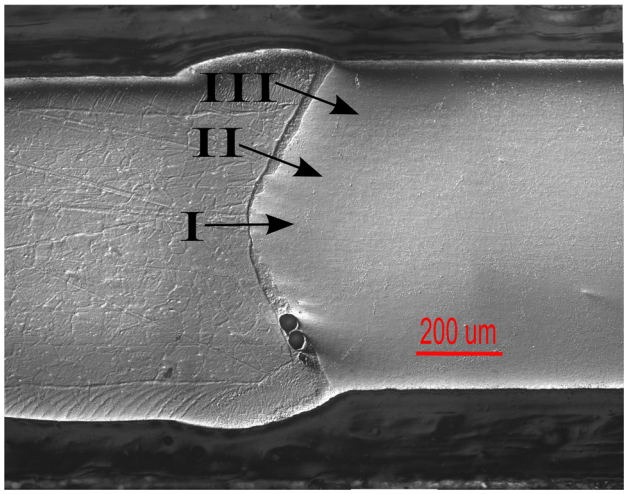

Fig. 8 Longitudinal section image of a 120 deg cone processed at a power of 15 W. The arrows indicate the paths of EDX line scans.

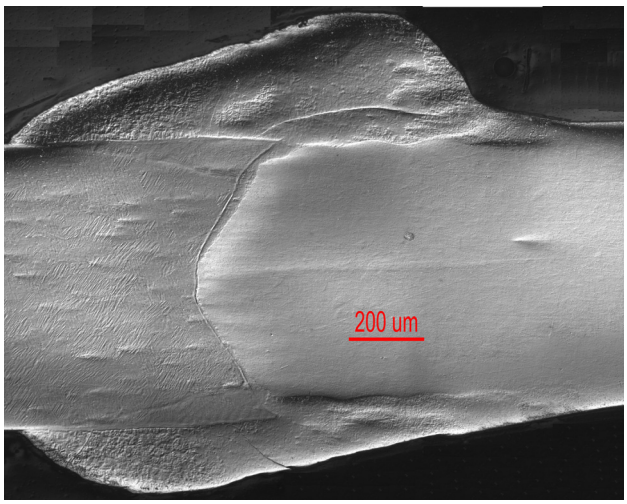

Fig. 9 Longitudinal section image of a 120 deg cone processed at a power of 17 W. Excessive melting and deformation is present on the outer surface.

distance. It takes very little heat to melt these thin walls, which may result in the apparently larger melted region of the 90 deg wires.

Longitudinal section images of samples from 15 W and 17 W are presented in Figs. 8 and 9. In both of the images, the cup and cone geometry is still intact. Along the angles of the interface, a possibly mixed region is visible. These regions will be analyzed via EDX. In the 15 W wire, joining is apparent throughout the center of the wire. But within the mixed region, two large circular defects are present. Also, joining is not apparent at the apex of the cone. This region will act as an initial crack during tensile testing, resulting in a lower fracture strength. The apex of the 17 W wire also does not appear to have complete joining, yet excessive deformation occurred on the outside. Therefore, continuing to increase the power will not result full joining of the interface. Alternatively, varying other parameters, such as angular velocity, could help to achieve more melting at the apex.

Composition. The width of the mixed region, where brittle intermetallics will form, is critical to the fracture strength of each joint. Typical results for wires irradiated at 13 W and 15 W are analyzed. EDX line profiles were acquired along arrows I, II, and III indicated in Fig. 8. The distance between scan points is 0.34 μm.

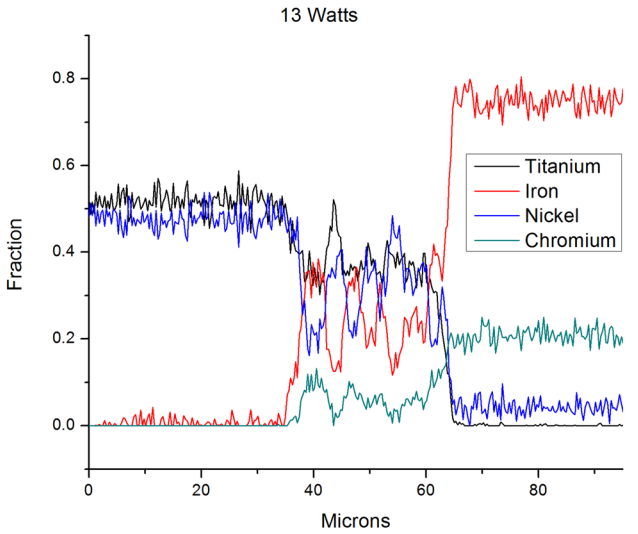

Fig. 10 EDX line scan across line II, indicating the mixing occurring in the joint. Sample irradiated at 13 W.

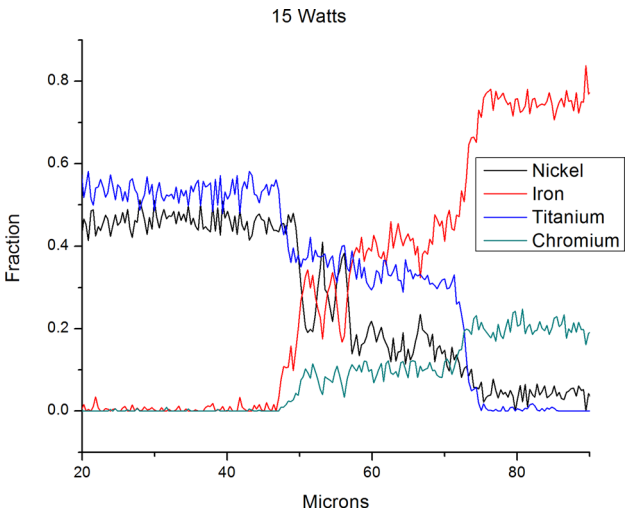

Fig. 11 EDX line scan across region II indicated in Fig. 8. Gradual decrease of concentration across the width of the interface is indicative of diffusion. Sample irradiated at 15 W.

Electron beam parameters were adjusted so that a detection rate of 1500 counts/s was achieved. A line profile for II is displayed in Fig. 10. The region from 37 μm to 65 μm is where mixing of the NiTi and stainless steel occurred. All of the scans along II and III for both power levels had very similar shape, with just the width of this mixing layer being the only difference. An abrupt transition happens between the mixed region and the base materials. To determine which phases are forming, we compare the compositions to the ternary phase diagram of Fig. 1. Since it does not appear on the phase diagram, the amount of chromium is neglected, which will slightly increase the concentrations from those displayed on the line scan. Two peaks stand out: one where titanium reaches nearly 50% and the other where nickel reaches nearly 50%. For both of these, the iron level is between 10% and 20%. Comparison with the phase diagram indicates that these are regions of (Fe,Ni)Ti.

The widest mixing zone occurred on II for the wire processed at 15 W shown in Fig. 11, with a width of 33 μm. Instead of having a flat trend along the length, this joint has more of a slow transition from the NiTi to the stainless steel. This is evidence that

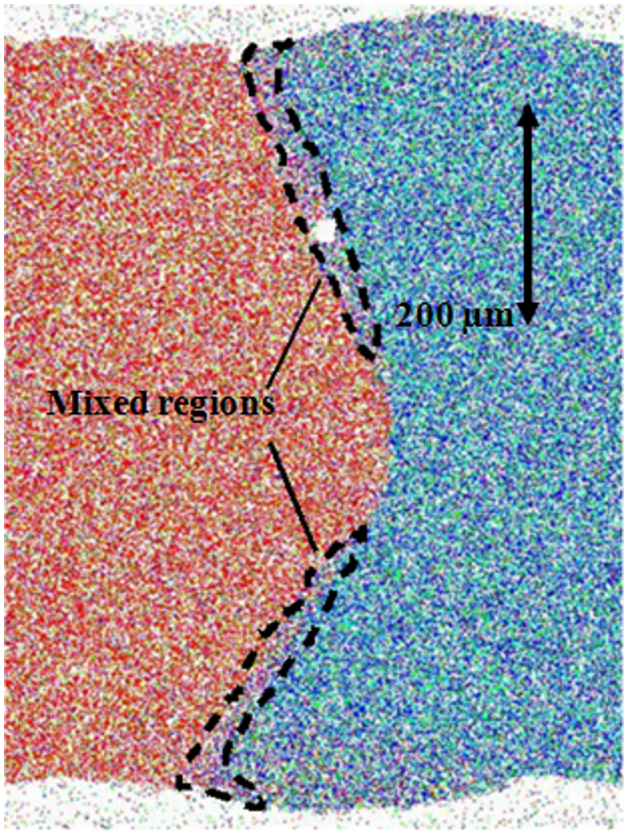

Fig. 12 EDX compositional map, corresponding to the longitudinal sectioned image of Fig. 8, showing iron (red) left of the mixed region; nickel (green) and titanium (blue) are to the right of the mixed region. Laser power is 15 W. A mixing region is observed along the interface, the width of which decreases toward the center of the wire. This indicates that the lighter colored regions along the interface of the longitudinal sectioned images are indeed the mixed regions.

diffusion of the materials has taken place. The thinnest mixing zone occurred on II for the wire processed at 13 W, with a width of only 18 μm. Analysis on I for both samples showed no mixing zone, indicating that joining did not occur at the centers. As is expected, the mixing for the 13 W sample is consistently lower than that of the 15 W.

Figure 12 displays an EDX area scan of the sample from Fig. 8. Within the areas indicated as the mixed region, we see iron, nickel, and titanium. This mixed region corresponds to the lighter colored region visible along the interface in Fig. 8. From this, it is apparent that joining did not occur along the entire interface for these processing parameters.

Joint Strength. Different rotation speeds have different laser interaction times, so slower rotations allow for more heat input. But at the same time, slower rotation speeds also allow for more heat to be conducted away, resulting in lower interface temperatures. Characterizing the laser parameters by the total amount of energy input (power $\times$ time), is unable to capture both of these effects [41]. As such, strengths for different rotation speeds are plotted separately as a function of power. The average load at fracture for a sample of wires processed at a rotation speed of 3000 deg/s is presented in Fig. 13. For both the 90 deg and 120 deg wires, an upward trend with power is evident. Also, as the power increases the variance in tensile strength decreases. This higher consistency is attributed to the excess melting that occurs under the higher powers. When the wires are being rotated under the laser, there is some slight unavoidable alignment error. At

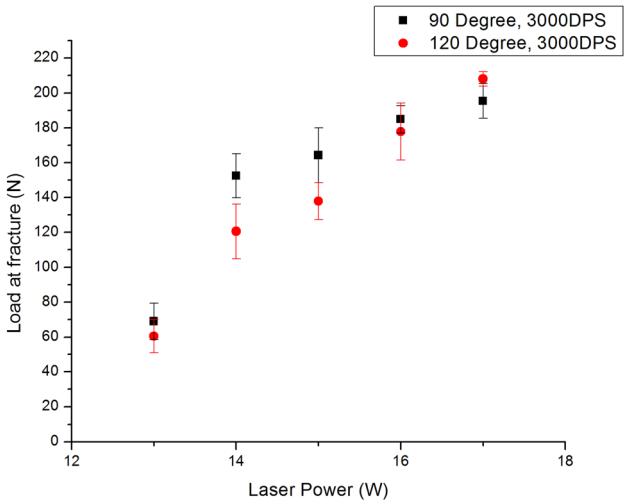

Fig. 13 Increase of load at fracture with increasing laser power input. Standard error for each level is indicated. Note that the 90 deg wires are stronger than the 120 deg wires at every power except for 17 W.

17 W, the large melt pool is able to fill in the gaps that are not perfectly aligned. This does not occur at the lower power levels, and thus they will be more sensitive to the alignment. For 13 W–16 W, the 90 deg angle wires have higher average fracture strength than the 120 deg angle wires. This is consistent with the idea that increasing the interface surface area will allow for higher fracture loads. But, at 17 W, the 120 deg wires have a higher average load. It is possible that at this higher power, the increased surface area allowed for more formation of brittle intermetallic phases.

The axial load causes the cross sectional area of the joint to increase during processing. This effect may cause some misinterpretation of Fig. 13. The loads at fracture for various rotation speeds have been normalized by the cross sectional area of the fracture, and are plotted in Fig. 14. Here, we see that the fracture strength will actually decrease with overheating. This is evidence that too much mixing occurs at the higher power levels, and therefore large amounts of brittle intermetallics are forming. At 3000 deg/s and 14 W, the 90 deg wires have an average strength of about 310 MPa, which is the highest level reached for this rotation speed. The highest strength of 270 MPa for the 120 deg wires occurs at 15 W. The ideal power level is where a minimum yet sufficient amount of melting occurs. With their sharper angle, the 90 deg wires overlap more than the 120 deg wires, resulting in better contact. The amount of melting at 14 W may be ideal to join the 90 deg wires together, but the 120 deg wires need slightly more melting in order to overcome some small misalignment effects.

In Fig. 14, the difference in strength between the 90 deg and 120 deg interfaces rotated at the slower velocities is much more pronounced than the wires irradiated at 3000 deg/s. From the thermal model, we know that the wires at higher rotation speeds reach higher temperatures. Thus, the strength results indicate that the samples at 3000 deg/s overmelt, mix, and negate the effect of the different interface angles. For the 2500 deg/s samples, the 90 deg wires irradiated at 14 W had an average fracture strength of 374 MPa, which is the highest level achieved. The highest level achieved for the 2000 deg/s samples of 342 MPa occurred at 15 W. The additional power necessary to reach the peak for the samples processed at slower rotational speeds is again consistent with the thermal model results presented in Fig. 5. Since the strongest samples fractured at levels below the lowest possible superelastic plateau of 480 MPa, no complex stress distributions are occurring at the interface from a phase transformation. The wires rotated at 2000 DPS have the longest interaction time with the laser. While the wires rotated at 3000 DPS have the fastest

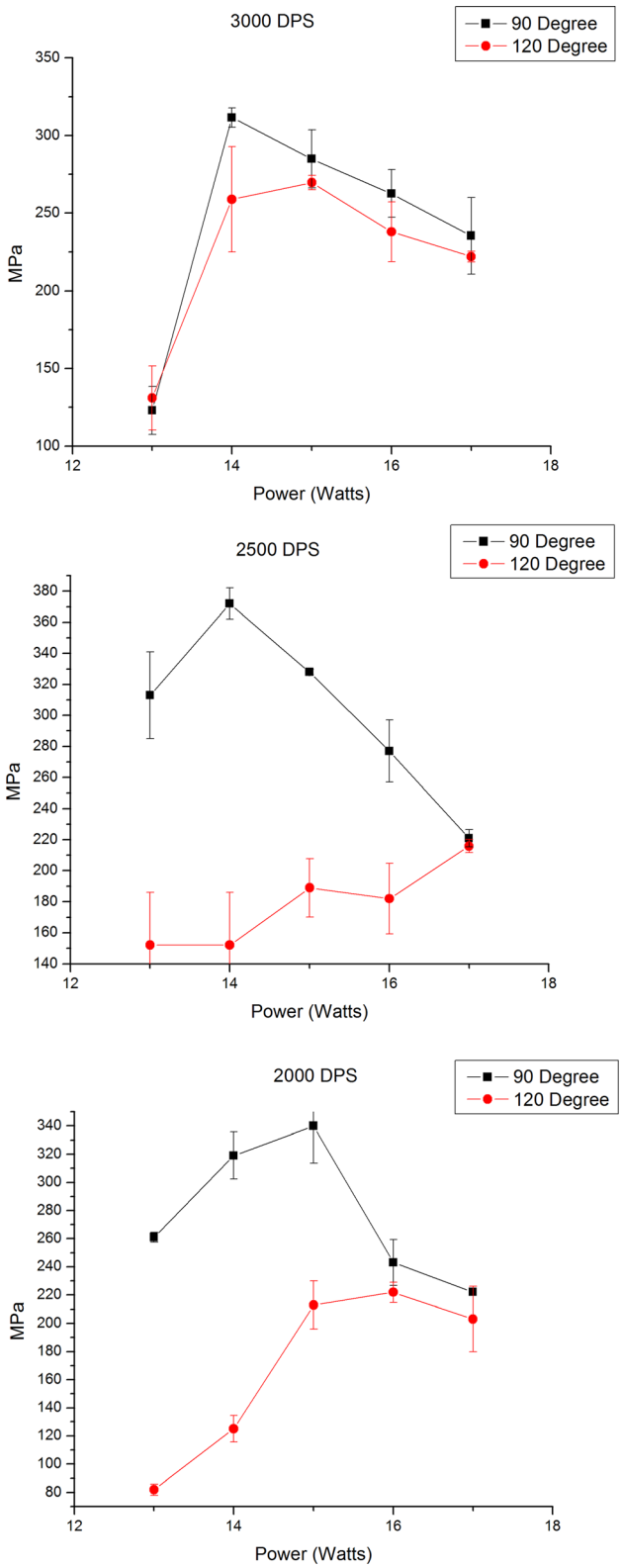

Fig. 14 Stress at fracture over a range of power levels. The 90 deg wires are consistently stronger than the 120 deg wires, which is consistent with predictions.

processing time, therefore less time for heat dissipation from conduction to occur. Yet, it is the 2500 DPS rotation that gives the strongest result, suggesting that at this rotation speed, the effects of total heat input and heat dissipation counteract each other in a beneficial way.

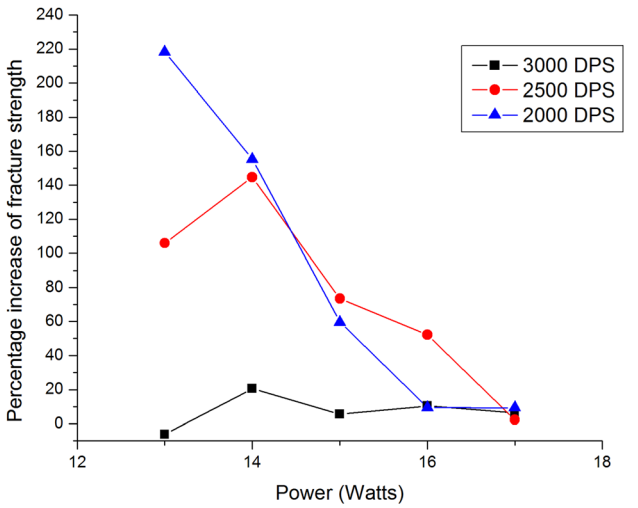

Fig. 15 Comparison of fracture strength between two different angles. The percentage scale on the left is how much stronger the 90 deg joint is compared to the 120 deg joint, for given power and angular velocities. As the power is increased, the difference between the two geometries reduces. This graph does not indicate which parameters gave the best overall results, but simply indicates the difference between the two angles.

For all power levels, aside from 13 W at 3000 deg/s, the 90 deg wires have the higher of the two strengths. This chart is normalized to cross sectional area, but the overall interface area of the 90 deg wires is still larger, indicating that increasing surface area due to different joint geometry can increase the fracture strength of these wire joints. It is noted that standard stainless steel 304 yields at 205 MPa. Clearly, the samples ran at 13–17 W are above this yield strength.

To compare the relative strengths between the two different apex angles, the percentage increase in strength from the 120 deg wires to the 90 deg wires, at each respective power level and rotation speed, has been plotted in Fig. 15. As previously indicated, the overmelting that occurs when the wires are rotated at 3000 deg/s dominates over the joint angle, resulting in minimal, if any, strength increase. The most pronounced difference in strength of the two geometries occurs at the lower powers. Since the percentage increase of fracture strength is significantly higher than the predicted difference in fracture toughnesses, clearly some other mechanisms are involved. The sharper angles on the 90 deg cones allow for the wires to slide deeper into each other with more overlap. Thus, upon rotation and before irradiation, the sharper angles stay in much better alignment. At the low powers, where melting is minimal, alignment plays a huge role in the strength of the joint. Any part of the interface that is not in contact with the other wire will not join. As the power is increased, the strength difference of the two geometries rapidly converges to zero. The overall strongest joint achieved (90 deg interface, 2500 deg/s rotation, 14 W) is about 150% stronger than the corresponding parameter for the 120 deg cone.

For comparison, the fracture strength of wires of the same diameter with a simple flat interface was also tested. These wires were held stationary, and irradiated at a power of 35 W as the laser was scanned toward the interface. Rotation of wires with flat interfaces was not viable, since the centrifugal force felt by the wires causes them to separate away from each other at the interface. As previously shown in the thermal model, rotation of the wires allows for more heating across the depth of the wires. Since the flat wires were not spun, more power input was required in order to achieve melting across the entire interface. The results are displayed in Fig. 16, with 180 deg corresponding to the flat interfaces. The rotated wires were spun at 2500 deg/s. We see that the

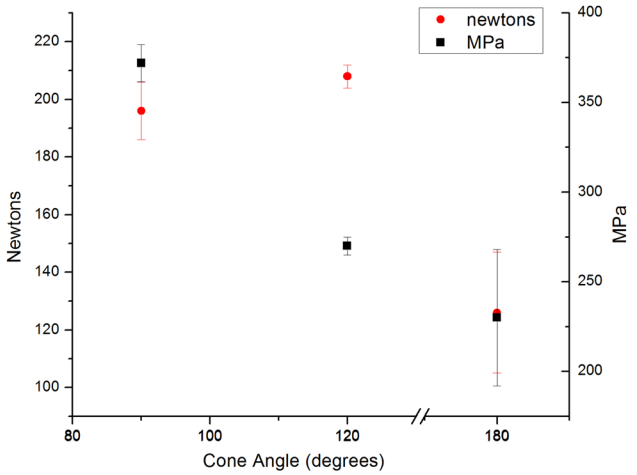

Fig. 16 Maximum average strength at fracture achieved for each wire geometry. Standard error is indicated. The 180 deg samples are the nonrotated, flat interfaces. Both of the conical wires have much higher fracture strengths.

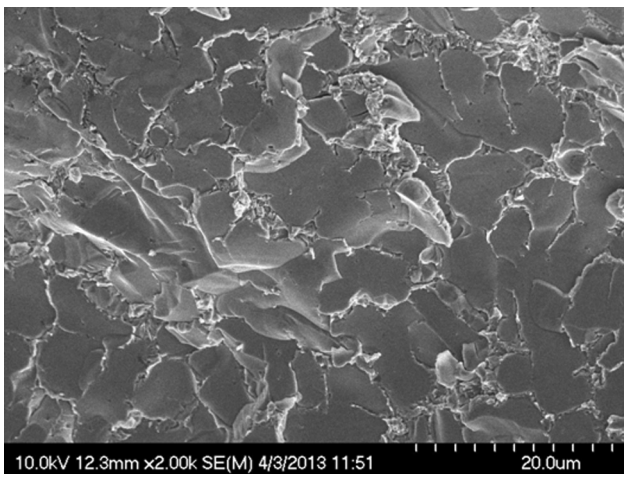

Fig. 17 Fracture surface indicating brittle transgranular fracture. 90 deg interface, 17 W, 3000 deg/s. Fractured at 200 MPa, along a surface not corresponding to the material interface.

wires that had the cup and cone geometry, and were rotated during irradiation, are indeed stronger than the nonrotated flat tests. The error for the rotated wires is also much smaller as well. During processing of the flat interfaces, the high laser power required to melt the bottom of the interface results in excessive melting of the top surface.

Fracture Surfaces. To better understand the differences of fracture strengths for various processing parameters, the fracture surfaces of a set of samples was analyzed via SEM. These images are presented in Figs. 17 and 18. Combining high laser power with fast rotation of the wires results in large amounts of melting at the interface, and thus a quite brittle joint. In Fig. 17, we see a large region of transgranular cleavage, with locally smooth fracture surfaces, which are indicative of brittle fracture. The fracture surface of this sample did not occur along the initial cup/cone geometry, but instead it occurred on a plane nearly perpendicular to the axis of loading. Overheating of this sample results in a large width of the interface. This wide interface gives a crack more opportunity to propagate through grains that are preferentially oriented to allow for low energy brittle fracture. Figure 18 is a sample irradiated at a lower power, but higher rotational speed.

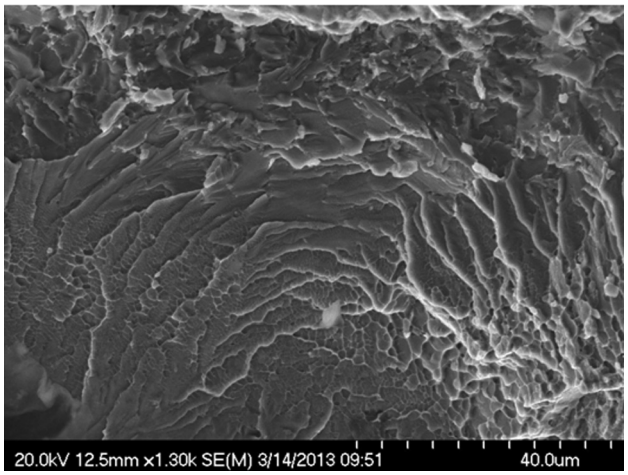

Fig. 18 Fracture surface of a sample that broke at 393 MPa, which was the highest strength achieved. The original cup and cone geometry was intact after fracture. Quasi-cleavage is apparent, indicating a better joint than Fig. 17.

With fracture occurring at 393 MPa, this was the strongest of all the samples.

When overheating does not occur, minimal changes are made to the base materials and thus fracture will be restricted to the brittle intermetallic interface. As is expected, fracture occurred along the conical geometry. Within this narrower interface, there will be a lower probability of a grain being preferentially oriented for low energy fracture. The majority of Fig. 18 is indicative of quasi-cleavage, which has characteristics of both brittle and ductile fracture. Some parabolic dimples are present in the lower right corner of the image, whose elongated shape is a result of the shear component along the interface.

Conclusion

The effect of using a cup and cone interfacial geometry for joining of NiTi-SS wires has been explored. Rotation of the wires during laser irradiation was used. This rotation produced much more uniform heating of the interface. Joints that had a 90 deg apex angle of the cone were found to consistently have higher fracture strengths than the 120 deg cones. The optimal laser power level for the 90 deg wires was 14 W, while 15 W for the 120 deg wires produced the strongest joints. Overmelting of the interface tended to negate the effects of the interfacial geometry. When overmelting did not occur, fracture was along the conical geometry. EDX analysis indicated (Fe,Ni)Ti formation in a thin region along the interface with a decreasing width toward the center of the wire. Even for the samples where excessive melting of the outside surface occurred, the apex of the cone in the center of the wires did not sufficiently melt. Thus, the effects on fracture strength that rotational velocity has been also explored. It was found that increasing the rotational speed resulted in increased melting. Even though cones with sharp apex angles are desirable with respect to the stress intensity formulation, limitations do exist for how small of apex angles can be used. Temperature uniformity will decrease as the apex angle is decreased. Also, the wall thickness of the NiTi cupped wires will decrease with sharper angles. These thin walls will be more sensitive to overheating, and also may fracture from shear loads that may be applied.

Acknowledgment

The authors acknowledge financial support from Columbia University and NSF under GOALI Award CMMI-1130564. Use of characterization equipment in the Shared Materials Characterization Laboratory, Columbia University, is also acknowledged.

References

[1] Duerig, T., Pelton, A., and Stöckel, D., 1999, "An Overview of Nitinol Medical Applications," Mater. Sci. Eng. A, **273–275**, pp. 149–160.

[2] Avery, R. E., 1991, "Pay Attention to Dissimilar-Metal Welds: Guidelines for Welding Dissimilar Metals," Chem. Eng. Prog., **4550**, pp. 1168–1177.

[3] Mubashar, A., Ashcroft, I. A., Critchlow, G. W., and Crocombe, A. D., 2011, "Strength Prediction of Adhesive Joints After Cyclic Moisture Conditioning Using a Cohesive Zone Model," Eng. Fract. Mech., **78**(16), pp. 2746–2760.

[4] Hand, H. M., Arah, C. O., McNamara, D. K., and Mecklenburg, M. F., 1991, "Effects of Environmental Exposure on Adhesively Bonded Joints," Int. J. Adhes. Adhes., **11**(1), pp. 15–23.

[5] Schubert, E., Zerner, D. I., and Sepold, P. G., "Laser Beam Joining of Material Combinations for Automotive Applications," Proc. SPIE, **3097**, pp. 212–221.

[6] Yamamoto, N., Liao, J., Watanabe, S., and Nakata, K., 2009, "Effect of Intermetallic Compound Layer on Tensile Strength of Dissimilar Friction-Stir Weld of a High Strength Mg Alloy and Al Alloy," Mater. Trans., **50**(12), pp. 2833–2838.

[7] Yan, Y., Zhang, D., Qiu, C., and Zhang, W., 2010, "Dissimilar Friction Stir Welding Between 5052 Aluminum Alloy and AZ31 Magnesium Alloy," Trans. Nonferrous Met. Soc. China, **20**, pp. s619–s623.

[8] Mathieu, A., Shabadi, R., Deschamps, A., Suery, M., Matteï, S., Grevey, D., and Cicala, E., 2007, "Dissimilar Material Joining Using Laser (Aluminum to Steel Using Zinc-based Filler Wire)," Opt. Laser Technol., **39**(3), pp. 652–661.

[9] Li, H., Sun, D., Gu, X., Dong, P., and Lv, Z., 2013, "Effects of the Thickness of Cu Filler Metal on the Microstructure and Properties of Laser-welded TiNi Alloy and Dtainless Steel Joint," Mater. Des., **50**, pp. 342–350.

[10] Satoh, G., and Yao, Y. L., 2011, "Laser Autogenous Brazing—A New Method for Joining Dissimilar Metals," Proceedings of the 30th International Congress on the Applications of Lasers and Electro-Optics, Lake Buena Vista, FL, pp. 315–324.

[11] Bao, J., and Yao, Y. L., 2001, "Analysis and Prediction of Edge Effects in Laser Bending," ASME J. Manuf. Sci. Eng., **123**(1), pp. 53–61.

[12] Schwartz, M., 1979, *Metals Joining Manual*, McGraw-Hill, New York.

[13] Brandal, G. B., Satoh, G., Yao, Y. L., and Naveed, S., 2013, "Effects of Interfacial Geometry on Laser Joining of Dissimilar NiTi to Stainless Steel Wires," Proceedings of MSEC 2013, Madison, WI.

[14] Otsuka, K., and Ren, X., 2005, "Physical Metallurgy of Ti–Ni-Based Shape Memory Alloys," Prog. Mater. Sci., **50**(5), pp. 511–678.

[15] Westbrook, J. H., 1967, "Historical Sketch," *Intermetallic Compounds*, J. H. Westbrook, ed., Robert E. Krieger Publishing Co., Inc., New York, pp. 3–14.

[16] Keyzer, J. D., 2008, *Thermodynamic Modeling of the Fe-Ni-Ti System: A Multiple Sublattice Approach*," Ph.D. thesis, University of Leuven, Leuven, Belgium.

[17] Vannod, J., 2011, "Laser Welding of Nickel-Titanium and Stainless Steel Wires: Processing, Metallurgy and Properties," Ph.D. thesis, Ecole Polytechnique Federale De Lausanne, Lausanne, Switzerland.

[18] Sauthoff, G., 1995, *Intermetallics*, VCH Publishers, New York.

[19] Martins, T. B., and Rechenberg, H. R., 2006, "Antiferromagnetic TiFe2 in Applied Fields: Experiment and Simulation," Hyperfine Interact., **169**, pp. 1273–1277.

[20] Ghosh, M., and Chatterjee, S., 2002, "Characterization of Transition Joints of Commercially Pure Titanium to 304 Stainless Steel," Mater. Charact., **48**(5), pp. 393–399.

[21] Eijk, C. V. D., Fostervoll, H., Sallom, Z. K., and Akselsen, O. M., 2003, "Plasma Welding of NiTi to NiTi, Stainless Steel and Hastelloy C276," ASM Materials Solutions 2003 Conference, Pittsburgh, PA.

[22] Borrisutthekul, R., Yachi, T., Miyashita, Y., and Mutoh, Y., 2007, "Suppression of Intermetallic Reaction Layer Formation by Controlling Heat Flow in Dissimilar Joining of Steel and Aluminum Alloy," Mater. Sci. Eng. A, **467**, pp. 108–113.

[23] Cacciamani, G., Keyzer, J. De, Ferro, R., Klotz, U. E., Lacaze, J., and Wollants, P., 2006, "Critical Evaluation of the Fe–Ni, Fe–Ti, and Fe–Ni–Ti Alloy Systems," Intermetallics, **14**(10–11), pp. 1312–1325.

[24] Ortega, A. M., Tyber, J., Frick, C. P., Gall, K., and Maier, H. J., 2005, "Cast NiTi Shape-Memory Alloys," Adv. Eng. Mater., **7**(6), pp. 492–507.

[25] Liu, Y., and McCormick, P. G., 1994, "Thermodynamic Analysis of the Martensitic Transformation in NiTi—Effect of Heat Treatment on Transformation Behaviour," Acta Metall. Mater., **42**(7), pp. 2401–2406.

[26] Satoh, G., Brandal, G. B., Naveed, S., and Yao, Y. L., 2013, "Laser Autogenous Brazing of Biocompatible, Dissimilar Metals in Tubular Geometries," Proceedings of North American Manufacturing Research Institution/SME, Vol. 41, Madison, WI.

[27] Vaidya, W. V., Horstmann, M., Ventzke, V., Petrovski, B., Koçak, M., Kocik, R., and Tempus, G., 2010, "Improving Interfacial Properties of a Laser Beam Welded Dissimilar Joint of Aluminium AA6056 and Titanium Ti6Al4V for Aeronautical Applications," J. Mater. Sci., **45**(22), pp. 6242–6254.

[28] Vaidya, W. V., Horstmann, M., Ventzke, V., Petrovski, B., Koçak, M., Kocik, R., and Tempus, G., 2009, "Structure-Property Investigations on A Laser Beam Welded Dissimilar Joint of Aluminium AA6056 and Titanium Ti6Al4V for Aeronautical Applications Part I: Local Gradients in Microstructure, Hardness and Strength," Materialwiss. Werkstofftech., **40**(8), pp. 623–633.

[29] Satoh, G., Yao, Y. L., and Qiu, C., 2013, "Strength and Microstructure of Laser Fusion-Welded Ti–SS Dissimilar Material Pair," Int. J. Adv. Manuf. Technol., **66**(1–4), pp. 469–479.

[30] Ogata, Y., Takatugu, M., Kunimasa, T., Uenishi, K., and Kobayashi, K. F., 2004, "Tensile Strength and Pseudo-Elasticity of YAG Laser Spot Melted Ti-Ni Shape Memory Alloy Wires," Mater. Trans., **45**(4), pp. 1070–1076.

[31] Hertzberg, R. W., 1996, *Deformation and Fracture Mechanics of Engineering Materials*, John wiley & Sons, Inc., New York.

[32] Awaji, H., and Kato, T., 1999, "Awaji—Criterion for Combined Mode I-II Brittle Fracture.Pdf," Mater. Trans., **40**(9), pp. 972–979.

[33] Munz, D., and Yang, Y. Y., 1992, "Stress Singularities at the Interface in Bonded Dissimilar Materials Under Mechanical and Thermal Loading," J. Appl. Math., **59**, pp. 857–861.

[34] Wah, T., 1976, "Plane Stress Analysis of a Scarf Joint," Int. J. Solids Structures, **12**, pp. 491–500.

[35] Ifflander, R., 2001, *Solid-State Lasers for Materials Processing*, Springer-Verlag, New York.

[36] Xie, J., Kar, A., Rothenflue, J. A., and Latham, W. P., 1997, "Temperature-Dependent Absorptivity and Cutting Capability of CO_2, Nd: YAG, and Chemical Oxygen-Iodine Lasers," J. Laser Appl., **9**, pp. 77–85.

[37] Bel'skaya, E. A., 2005, "An Experimental Investigation of the Electrical Resistivity of Titanium in the Temperature Range From 77 to 1600 K," High Temp., **43**(4), pp. 546–553.

[38] Incropera, F. P., and DeWitt, D. P., 2002, *Fundamentals of Heat and Mass Transfer*, John wiley & Sons, Inc., Hoboken, NJ.

[39] Younglove, B. A., and Hanley, J. M., 1986, "The Viscosity and Thermal Conductivity Coefficients of Gaseous and Liquid Argon," J. Phys. Chem. Ref. Data, **15**(4), pp. 1323–1337.

[40] "ASTM Standard E8, 2011, "Standard Test Methods for Tension Testing of Metallic Materials," ASTM International, West Conshohocken, PA."

[41] Li, W., and Yao, Y. L., 2001, "Laser Forming With Constant Line Energy," Int. J. Adv. Manuf. Technol., **17**(3), pp. 196–203.